Theoretical and Experimental Analyses of Photovoltaic Systems With Voltage- and Current-Based Maximum Power-Point Tracking

Mohammad A. S. Masoum, Hooman Dehbonei, and Ewald F. Fuchs, *Fellow, IEEE*

Abstract—Detailed theoretical and experimental analyses are presented for the comparison of two simple, fast and reliable maximum power-point tracking (MPPT) techniques for photovoltaic (PV) systems: the voltage-based (VMPPT) and the current-based (CMPPT) approaches. A microprocessor-controlled tracker capable of online voltage and current measurements and programmed with VMPPT and CMPPT algorithms is constructed. The load of the solar system is either a water pump or resistance. "Simulink" facilities are used for simulation and modeling of the novel trackers. The main advantage of this new MPPT, compared with present trackers, is the elimination of reference (dummy) cells which results in a more efficient, less expensive, and more reliable PV system.

Index Terms—Maximum power, photovoltaic, pump, tracker.

I. INTRODUCTION

PHOTOVOLTAIC (PV) systems find increased use in electric power technologies. The main drawbacks of PV systems are high fabrication cost and low energy-conversion efficiency, which are partly caused by their nonlinear and temperature-dependent V–I and P–I characteristics. To overcome these drawbacks, three essential approaches can be followed:

1) Improving manufacturing processes of solar arrays: many research efforts have been performed with respect to materials and manufacturing of PV arrays [1]–[3].
2) Controlling the insolation input to PV arrays: the input solar energy is maximized using sun-tracking solar collectors [4]–[6] or rearranging the solar-cell configurations of PV arrays with respect to changes in environmental conditions [7], [8].
3) Utilization of output electric power of solar arrays: the main reasons for the low electrical efficiency are the nonlinear variations of output voltage and current with solar-radiation levels, operating temperature, and load current. To overcome these problems, the maximum power operating point of the PV system (at a given condition) is tracked using online or offline algorithms and the system operating point is forced toward this optimal condition [9]–[19].

Many MPPT techniques have been proposed, analyzed, and implemented. They can be categorized as

A) "Look-up table" methods [9]–[11]—The nonlinear and time-varying nature of solar cells and their great dependency on radiation and temperature levels as well as degradation (aging, dirt) effects, make it difficult to record and store all possible system conditions.

B) "Perturbation and observation (P&O)" methods [12]–[14]—Measured cell characteristics (current, voltage, power) are employed along with an online search algorithm to compute the corresponding maximum power point independent of insolation, temperature, or degradation levels. Problems with this approach are undesirable measurement errors (especially for current) which strongly affects tracker accuracy.

C) "Computational" methods [15]–[19]—The nonlinear V–I characteristics of solar panel is modeled using mathematical equations or numerical approximations. The model must be valid under different insolation, temperature, and degradation conditions. Based on the modeled V–I characteristics, the corresponding maximum power points are computed for different load conditions as a function of cell open-circuit voltages or cell short-circuit currents.

In this paper, two simple and powerful maximum power-point tracking techniques (based on "computational" methods) known as voltage-based VMPPT [18] and current-based CMPPT [19] are simulated, constructed, and compared. Theoretical and experimental results illustrate the advantages and shortcomings of both techniques. Finally, the optimal applications of each tracker are classified.

II. RADIATION- AND TEMPERATURE-DEPENDENT SOLAR CELL CHARACTERISTICS

The nonlinear V–I and P–I characteristics of solar cells are well known [1]–[3]. Using the equivalent circuit of Fig. 1, the nonlinear V–I characteristics of M parallel strings with N series cells per string is

$$v_{PV} = \frac{N}{\lambda} \ln\left(\frac{I_{sc} - i_{pv} + MI_0}{MI_0}\right) - \frac{N}{M}R_s i_{pv} \qquad (1)$$

where I_{sc} is the cell short-circuit current (representing insolation level), I_0 is the reverse saturation current, R_s is the series
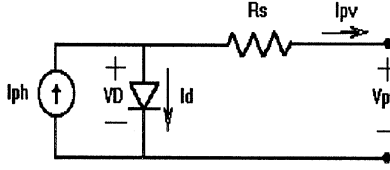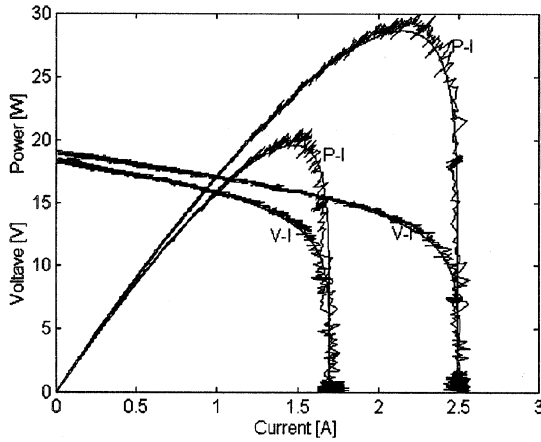
Fig. 1. Equivalent circuit of PV solar cell.

TABLE I
SPECIFICATIONS OF SILICON SOLAR PANELS (MANUFACTURED BY OFFC)

Current Temp. Coefficient	$\alpha = 0.002086$	[A/°C]
Voltage Temp. Coefficient	$\beta = 0.0779$	[V/°C]
Reverse Saturation Current	$I_0 = 0.5 \times 10^{-4}$	[A]
Short Circuit Cell Current	$I_{ph} = I_{SC} = 2.926$	[A]
Cell Resistance	$R_s = 0.0277$	[Ω]
Cell Material Coefficient	$\lambda = 0.049$	[1/V]

Fig. 2. Computed (2) and measured nonlinear *V–I* and *P–I* characteristics of one OFFC silicon solar panel (Table I).

cell resistance, and λ is a constant coefficient and depends upon the cell material.

For the silicon solar panel ($M = 1, N = 36$) used for the theoretical and experimental analyses of this paper [Table I, manufactured by the Iranian Optical Fiber Fabrication Co. (OFFC)], (1) can be written as

$$v_{pv} = 1.767 \ln \left(\frac{I_{sc} - i_{pv} + 0.000\,05}{0.000\,05} \right) - i_{pv}. \qquad (2)$$

Computed (2) and measured *V–I* as well as *P–I* characteristics for the OFFC panel are shown in Fig. 2 for two insolation levels. This figure illustrates the variations of the cell maximum power point (e.g., the maximum of the *P–I* curves) with respect to insolation levels.

Unfortunately, there also exists for the *V–I* characteristics a nonlinear relationship with respect to temperature. Considering the impact of temperature variation [3], (2) will have different coefficients for different temperatures at the same insolation level

$$v_{pv} = 1.69 \ln \left(\frac{3.005 - i_{pv} + 0.000\,24}{0.000\,24} \right) - i_{pv} \qquad (3a)$$
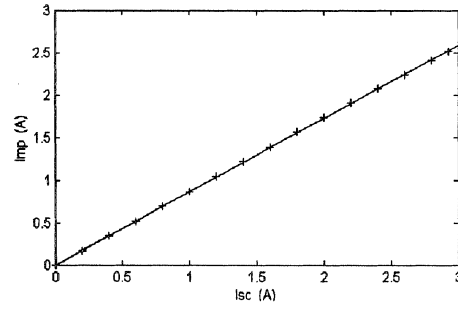
Fig. 3. Computed ("+" signs) and linear (4) dependence of "cell current corresponding to maximum power" versus "cell short-circuit current" for one OFFC panel ($T = 25\,°C$ at varying insolation levels).
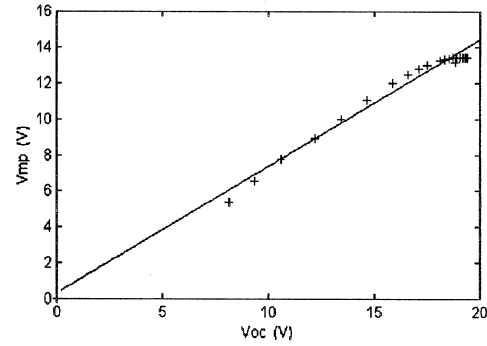
Fig. 4. Computed ("+" signs) and linear (5) dependence of "cell voltage corresponding to maximum power" versus "cell open-circuit voltage" for one OFFC panel ($T = 25\,°C$ at varying insolation levels).

$$v_{pv} = 1.82 \ln \left(\frac{2.83 - i_{pv} + 0.000\,01}{0.000\,01} \right) - i_{pv}. \qquad (3b)$$

Equations (3a) and (3b) are evaluated for one OFFC panel at $T = 70°C$ and $T = -20°C$, respectively.

Equations (2) and (3) along with Fig. 2 depict the strong nonlinear dependency of maximum power point (MPP) with respect to insolation and temperature levels and justify for any highly efficient PV system an accurate MPP tracker.

III. VOLTAGE- AND CURRENT-BASED MPPT TECHNIQUES

To determine the operating point corresponding to maximum power for different insolation levels, (2) is used to compute the partial derivative of power with respect to cell current. Reference [19] employs numerical methods to show a linear dependence between the "cell currents corresponding to maximum power" and the "cell-short circuit currents"

$$I_{MP} = M_C I_{SC}. \qquad (4)$$

This equation characterizes the main idea of the current-based maximum power-point tracking (CMPPT) technique. M_C is called the "current factor" and is equal to 0.86 for the OFFC silicon panel (Table I). Equation (4) is plotted in Fig. 3 together with the computed (almost linear) dependence of I_{MP} with respect to I_{SC} (indicated by "+" signs).

A similar approach is taken in [17]. It is shown that "cell voltages corresponding to maximum power" exhibit a linear dependence, independent of panel configuration, with respect to cell
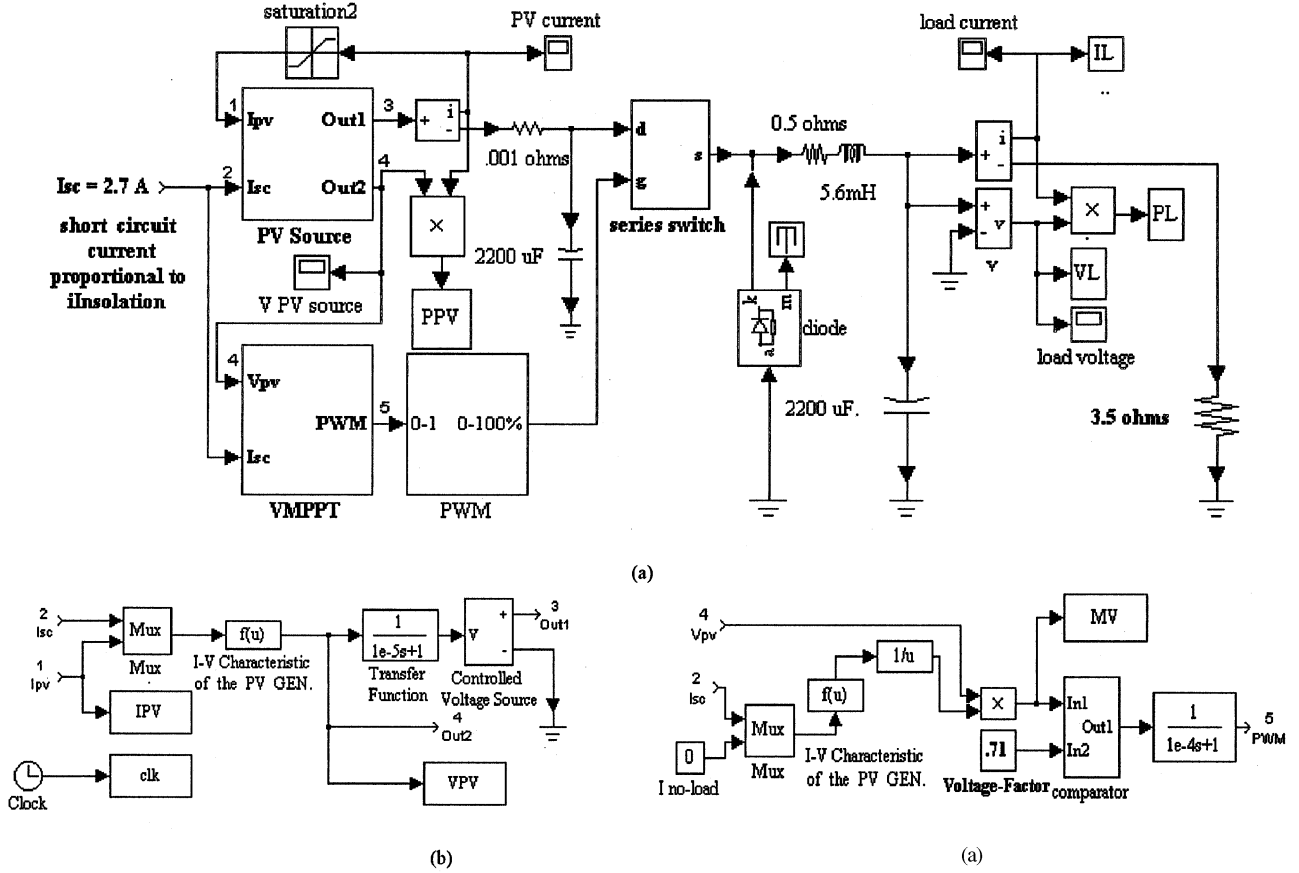
Fig. 5. Simulation of a resistive-load PV system with VMPPT (in buck mode): (a) circuit diagram; (b) detail of "PV source" block; and (c) detail of "VMPPT" block.

"open-circuit voltages" for different insolation and temperature levels

$$V_{MP} = M_V V_{OC}. \tag{5}$$

This equation represents the concept of the voltage-based maximum power-point tracking (VMPPT) technique and M_V, which is called the "voltage factor," is equal to 0.71 for the OFFC silicon panel. Equation (5) is plotted in Fig. 4 along with the computed (almost linear) dependence. According to Figs. 3 and 4, CMPPT and VMPPT techniques are simple and fast methods for maximum power-point estimation.

IV. SIMULATION OF VMPPT AND CMPP TECHNIQUES

Simulink software and its facilities are used to model a resistive-load solar system with a VMPPT (in buck mode) tracker as shown in Fig. 5(a).

For the solar cell equivalent circuit, we have created a block called "PV source" as shown in Fig. 5(b), which simulates the nonlinear *V–I* characteristics of one OFFC panel (2), employing the cell short circuit (Isc) as a measure of insolation level. We have introduced a delay function to limit the fast current response of the "controlled voltage source" and to improve the convergence of solution.

For the voltage-based PPT equivalent circuit, we have used a block call "VMPPT" as shown in Fig. 5(c). This block computes

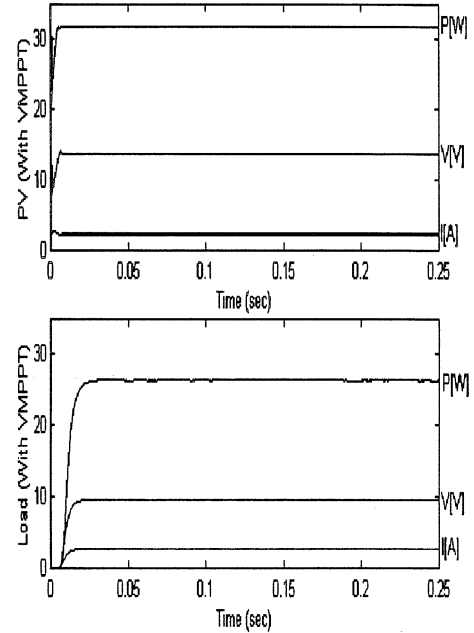Fig. 6. Computed (using Fig. 5) voltage, current, and power characteristics of the PV panel (top graph) and at the 3.5-Ω resistive-load (bottom graph) for the PV system with a buck-mode VMPPT. Compare these results with the corresponding measured characteristics of Fig. 11.

cell open-circuit voltage [using Isc and (2), compares it with the PV output voltage using (5) and calculates the firing commands
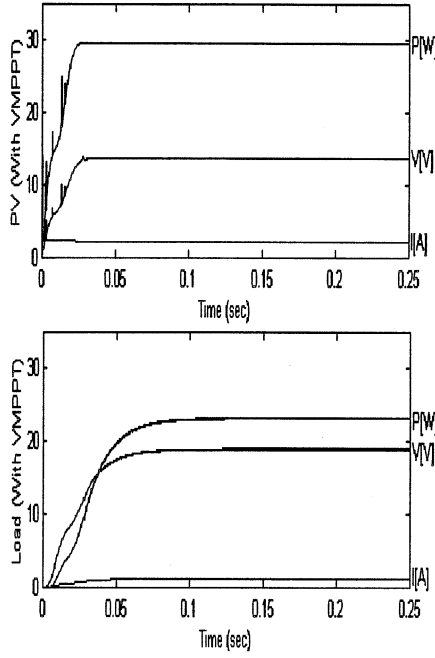
Fig. 7. Computed voltage, current, and power characteristics of the PV panel (top graph) and at the 15.5-Ω resistive-load (bottom graph) for the PV system with a boost-mode VMPPT. Compare these results with the corresponding measured characteristics of Fig. 13.

for the pulse-width- modulation (PWM) block]. We have also introduced a delay function for the same reason as in Fig. 5(b).

Fig. 6 shows computed voltage, current, and power characteristics of Fig. 5 at the output of the "PV source" block (top graph) and across the 3.5-Ω resistive load (bottom graph). There is good agreement between the computed (Fig. 6) and measured (Fig. 11) results for the resistive-load PV system with a VMPPT (in buck-mode) tracker. The captured maximum power is approximately 32 W.

For a boost mode of the buck/boost converter we deactivate the series switch (see Fig. 8) and activate the shunt switch, remove the diode, and place it after the inductor and increase the load resistance to 15.5 Ω. We can simulate and plot the results for a boost-mode VMPPT as shown in Fig. 7. The results are in good agreement with the corresponding measurements of Fig. 13. Similar results were obtained for PV systems with VMPPT and motor loads, as well as PV systems with CMPPT and resistive and motor loads.

V. CONSTRUCTION OF VMPPT AND CMPPT SYSTEMS

For the experimental comparison of VMPPT and CMPPT techniques, a microprocessor-based tracker (Fig. 8) with the following capabilities was constructed and used:

a) implementing VMPPT and CMPPT techniques;
b) continual control of dc/dc converter (buck or boost mode) according to the selected tracking method;
c) for a VMPPT tracker, online measurements of panel open-circuit voltage, estimation of panel maximum power points (5), and continuous matching of load operating point (e.g., by changing motor speed or adjusting resistor power) with panel maximum power condition;

d) for a CMPPT tracker: online measurements of panel short-circuit current, estimation of panel maximum power points (4), and continuous matching of load operating point with the panel maximum power condition.

The multipurpose MPP tracker, which is placed between the OFFC silicon panel and the selected load (resistive or water pump), consists of the following main parts (Fig. 8):

a) a series switch which is used for online measurement of panel open-circuit voltage. The sampling is done when the load is disconnected by the PWM command signal;
b) a shunt switch for online measurements of panel short-circuit current. This is done by sampling the voltage drop across a 5/80-Ω resistor during the time when PWM disconnects the load from the PV panel;
c) a dc/dc converter which can operate in buck or boost mode according to load requirements (e.g., a resistive load may operate in either mode, while a motor load usually operates in boost mode);
d) the driver circuitry is controlled by a microcontroller unit (MCU) [[18 Fig. 7]], which has the full responsibility of converter switching;
e) the 80C51 MCU [18] computes the command signals based on the selected conditions (e.g., VMPPT or CMPPT, buck or boost mode) and load characteristics. It consists of digital-to-analog and analog-to-digital converters (DACs) and (ADCs), switch drivers, power supplies, display, and keyboard. This MCU relies on measured information (e.g., panel output and open-circuit voltages or panel-output and short-circuit currents) and the selected tracking technique (e.g., VMPPT or CMPPT) to compute and send appropriate firing signals to converters and switches;
f) diodes D1 and D6 which operate according to user requirements. For example, for a VMPPT in boost mode only D6 conducts. For a CMPPT in buck mode, only D1 operates and for CMPPT in boost mode, both diodes will have to conduct. The voltage drop across each diode is approximately 0.8 V.

The circuit of Fig. 8 is an experimental setup, with relatively high circuit losses designed for the comparison of VMPPT and CMPPT algorithms. In actual trackers, only one tracking technique is employed and many parts of this experimental circuit are not required.

VI. MEASURED CHARACTERISTICS OF VMPPT AND CMPPT

In order to investigate the performance of VMPPT and CMPPT techniques under different operating and load conditions, the tracker of Fig. 8 was used with resistive loads as well as motor loads with and without the selected MPP tracker.

Fig. 9 shows the measured *V–I* and *P–I* characteristics for typical insolation and temperature levels (e.g., operating conditions of Figs. 11 and 12). The impact of voltage factor (M_V) variations is measured and plotted in Fig. 10, which confirms the unique value of $M_V = 0.71$ for OFFC silicon panels as reported in [17].

Fig. 8.   Constructed multipurpose microprocessor-based tracker used for the analysis and comparison of VMPPT and CMPPT techniques.

Fig. 9.   Measured V–I and P–I characteristics corresponding to the operating conditions (insolation and temperature levels) of Figs. 11 and 12.

Fig. 10.   Comparison of measured panel output power (resistive-load $R = 3.5\ \Omega$) for different voltage factors using VMPPT (at constant insolation level).

A. Resistive Loads

Fig. 11 displays measured voltage, current, and power characteristics at the output of the solar panel as well as at the input

of the resistive load ($R = 3.5\ \Omega$) with and without VMPPT (in buck mode). Comparing these time functions with the corresponding computed characteristics of Fig. 6, we notice good agreement under transient and steady-state conditions.

Fig. 12 shows similarly measured characteristics under the same insolation and load conditions using the CMPPT technique. As expected and reported in [18], [19], both techniques estimate the panel maximum power resulting in considerable increases of PV output power (e.g., approximately 20% and 10% for VMPPT and CMPPT, respectively) and system-output power (e.g., about 12.5% and 4% for VMPPT and CMPPT, respectively). Considerable power losses are due to the multipurpose tracker (Fig. 8), designed to evaluate VMPPT and CMPPT algorithms. The zero power readings on the measured characteristics (e.g., at $t = 0.17$ s and $t = 0.08$ s in Figs. 11 and 12, respectively) correspond to the online open-circuit voltage or online short-circuit current measurements of the solar panel.

B. Motor Load

A solar water pump was constructed by replacing the resistive load of Fig. 8 with a small permanent magnet dc motor (24 V, 45 W) coupled with a centrifugal pump. Figs. 14 and 15 demonstrate the measured time functions for VMPPT and CMPPT tracking procedures, respectively. Analyses of these graphs indicate

a) The insolation levels of the two experiments are not the same, which results in different PV maximum powers (e.g., approximately 32.5 W in Fig. 14 and 34 W in Fig. 15).

b) The zero-power instants indicate PV panel open-circuit voltage (e.g., at $t = 0.22$ s in Fig. 14) or its short-circuit current measurements (e.g., at $t = 0.11$ s in Fig. 15).
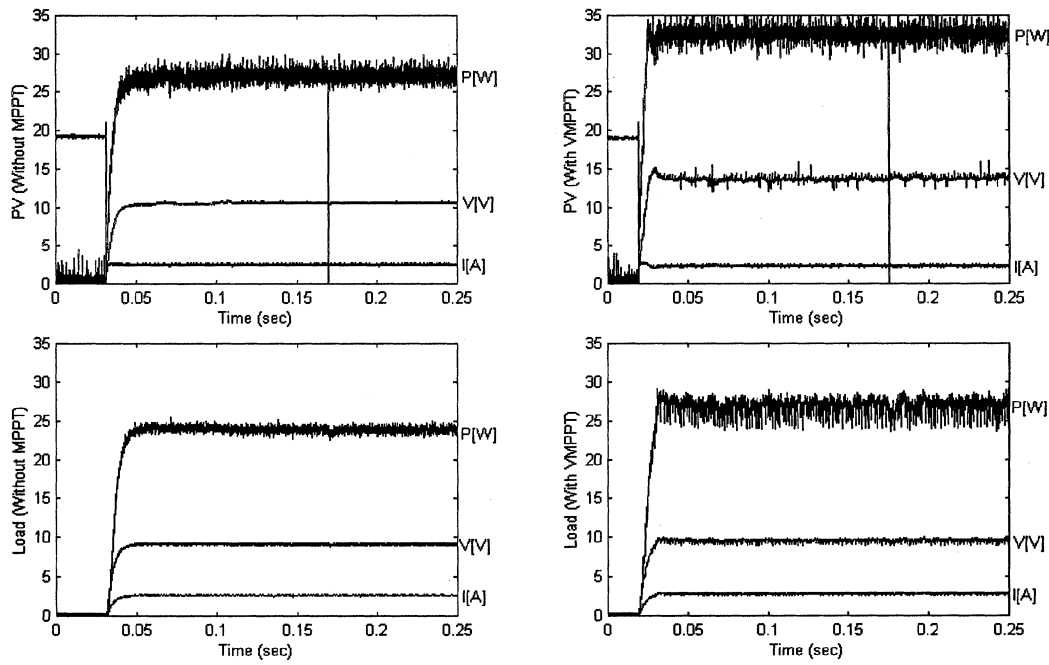
Fig. 11. Measured time functions of voltage, current, and power at the output of the solar panel and at the input of the resistive-load ($R = 3.5 \ \Omega$) with and without VMPPT (in buck mode). Compare these with the corresponding computed characteristics of Fig. 6.
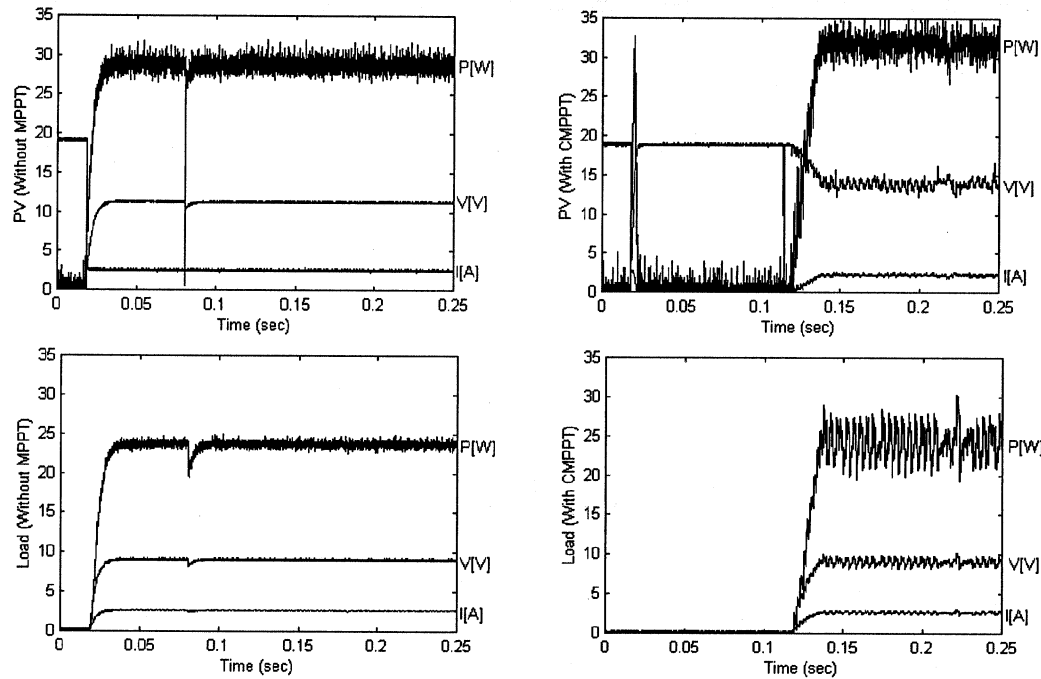

Fig. 12. Measured time functions of voltage, current, and power at the output of the solar panel and at the input of the resistive load ($R = 3.5 \ \Omega$) with and without CMPPT (in buck mode).

c) Comparing the left and rightside graphs, one notes the fine tracking performance of both methods which results in considerable increases in the panel output power (about 41%) as well as in the overall system output power (approximately 30%).

d) Circuit losses are larger for the CMPPT system of Fig. 15, e.g., approximately $(34 - 22.5)$W $= 11.5$ W, compared with the VMPPT system of Fig. 14, e.g., about $(32.5 -$

$25)$W $= 7.5$ W. This is due to the complicated nature of CMPPT hardware.

e) As expected, the output time functions of the dc motor are distorted due to commutation. The presence of a maximum power-point tracker (especially CMPPT) results in considerably larger waveform distortion due to PWM and online voltage and current sampling and amplification.
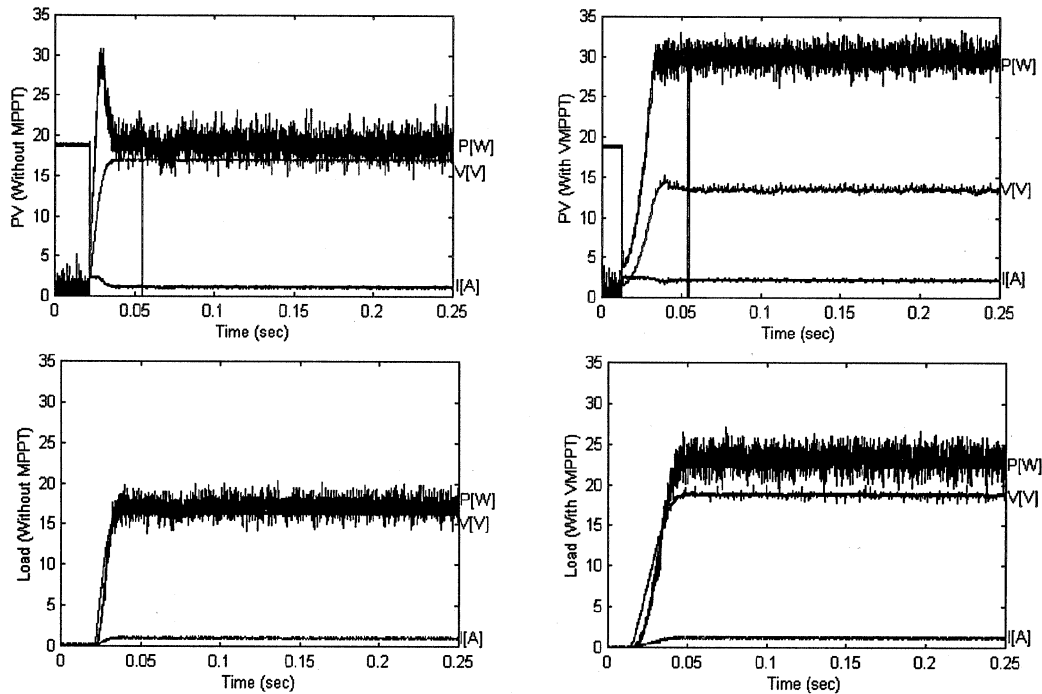
Fig. 13.   Measured time functions of voltage, current, and power at the output of the solar panel and input of the resistive load ($R = 15.5 \ \Omega$) with and without VMPPT (in boost mode). Compare these with the corresponding computed plots of Fig. 7. The insolation levels of Figs. 9 and 13 are different.

f) During motor starting, the system maximum power point is instantly passed and recorded. This is due to the starting characteristics of a dc motor, initially forcing the system operating point in the "constant current" region of panel *V–I* characteristics.

g) The presence of a MPP tracker increases the (system) time constant (especially for CMPPT systems), this is due to the variation of the system equivalent resistance.

By increasing the load resistance (e.g., from 3.5 to 15.5 Ω), we can measure the characteristics of a VMPPT tracker in boost mode (Fig. 13). These results indicate an increase of approximately 37% in PV output power while the final output power across the load has improved by about 26%. In order to capture the panel maximum power, the system operating point is moved from the "constant current" region to the "constant voltage" region of the *V–I* characteristic. In this process, the cell (panel) maximum power point is instantly passed and recorded as shown on the top-left power graph of Fig. 13 (at $t = 0.025$ s). Compare these time functions with the corresponding computed plots of Fig. 7.

VII. COMPARISON OF VMPPT AND CMPPT TECHNIQUES

Based on the theoretical (Figs. 3–7) and experimental (Figs. 8–15) investigations of this paper, the following results may be stated.

- Both VMPPT and CMPPT techniques are fast, practical, and powerful methods for MPP estimation of PV generators under all insolation and temperature conditions; the resulting output powers are increased (e.g., 12.5, 4, 26, 30, and 31% in Figs. 11 and 12 and 13 and 14, respectively). The increase in output power depends on load character-

istics, environmental factors (insolation and temperature), and the type of tracker used.
- Both types of trackers may be used either with buck- or boost-type converters depending on the load characteristics.
- Online measurements of PV short-circuit and output currents make CMPPT hardware more complicated and expensive compared with (same rating) VMPPT circuitry, requiring voltage measurements only.

VIII. CONCLUSIONS

Two powerful and practical methods for maximum power-point tracking of PV systems are investigated and compared. For the theoretical analysis, "Matlab" and "Simulink" facilities are employed and a multipurpose microprocessor-based tracker, capable of implementing VMPPT and CMPPT techniques, is constructed and used. Based on the results presented before, the following conclusions may be stated.

- The linear current function used by the CMPPT technique is a more accurate approximation of the actual nonlinear PV characteristics compared with the linear voltage function of the VMPPT technique.
- VMPPT technique is naturally more efficient and has less circuit losses (especially for buck-mode trackers).

As a result, the optimal MPPT methodology strongly depends on matching load and tracker characteristics. Considering the natural behavior, advantage, and limitations of CMPPT and VMPPT techniques, the following suggestions are made for some typical PV loads:

- PV loads, which require low-voltage and high-current outputs (e.g., battery chargers and low-resistance loads), are
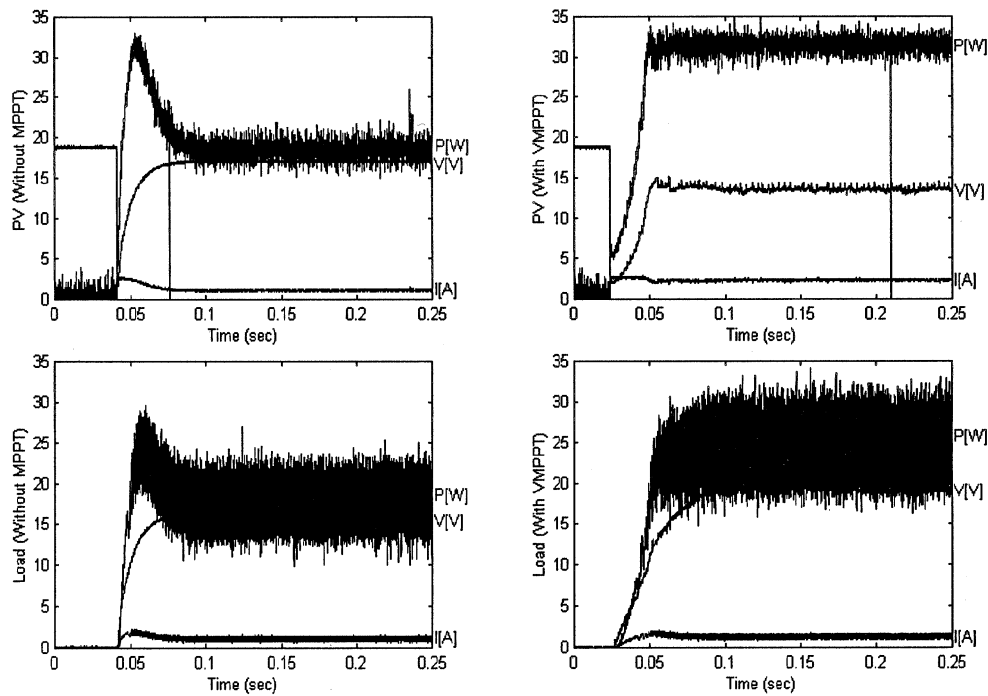
Fig. 14. Measured time functions of voltage, current, and power at the output of the solar panel and input of the dc motor (24 V, 45 W) with and without VMPPT (in boost mode).
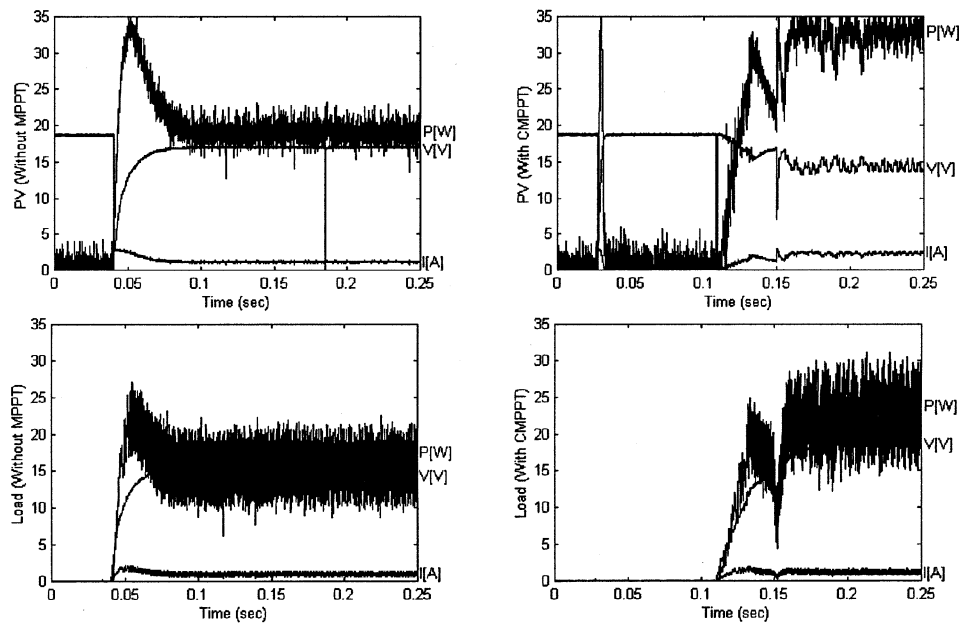

Fig. 15. Measured time functions of voltage, current, and power at the output of the solar panel and input of the dc motor (24 V, 45 W) with and without CMPPT (in boost mode).

best matched with the VMPPT system and result in better overall performance (cost, efficiency, and noise).

- PV loads with high voltage and low current (e.g., motors and high resistive loads) could be matched with either VMPPT or CMPPT systems, but the VMPPT technique will result in simple hardware with higher efficiency and lower noise and cost.

REFERENCES

[1] H. S. Rauschenbach, *Solar Cell Array Design Handbook: The Principles and Technology of Photovoltaic Energy Conversion*. New York: Van Nostrand, 1980.

[2] M. A. Green, *Solar Cells: Operating Principles. Technology and System Applications*. Englewood Cliffs, NJ: Prentice-Hall, 1982.

[3] Z. M. Salameh, B. S. Borowy, and A. R. A. Amin, "Photovoltaic module-site matching based on the capacity factors," *IEEE Trans. Energy Conversion*, vol. 10, pp. 326–332, June 1995.

[4] M. Buresch, *Photovoltaic Energy Systems Design and Installation*. New York: McGraw-Hill, 1983.

[5] J. S. Hsieh, *Solar Energy Engineering*. Englewood Cliffs, NJ: Prentice-Hall, 1986.

[6] R. O. Hughes, "Optimum control of sun tracking solar collectors," in *Proc. Annu. Meeting of Int. Solar Energy Soc.*, Denver, CO, Aug. 28–31, 1978.

[7] K. E. Yeager, "Electric vehicles and solar power: Enhancing the advantages of electricity," *IEEE Power Eng. Rev.*, vol. 12, Oct. 1992.

[8] M. M. Saied and M. G. Jaboori, "Optimal solar array configuration and dc motor field parameters for maximum annual output mechanical energy," *IEEE Trans. Energy Conversion*, vol. 4, pp. 459–465, Sept. 1989.

[9] T. Hiyama, S. Kouzuma, and T. Iimakudo, "Identification of optimal operating point of PV modules using neural network for real time maximum power tracking control," *IEEE Trans. Energy Conversion*, vol. 10, pp. 360–367, June 1995.

[10] ——, "Evaluation of neural network based real time maximum power tracking controller for PV system," *IEEE Trans. Energy Conversion*, vol. 10, pp. 543–548, Sept. 1995.

[11] T. Hiyama and K. Kitabayashi, "Neural network based estimation of maximum power generation," *IEEE Trans. Energy Conversion*, vol. 12, pp. 241–247, Sept. 1997.

[12] I. H. Altas and A. M. Sharaf, "A novel on-line MPP search algorithm for PV arrays," *IEEE Trans. Energy Conversion*, vol. 11, pp. 748–754, Dec. 1996.

[13] C. Hua, J. Lin, and C. Shen, "Implementation of a DSP-controlled photovoltaic system with peak power tracking," *IEEE Trans. Ind. Electron.*, vol. 45, pp. 99–107, Feb. 1998.

[14] J. H. R. Enslin and D. B. Snyman, "Combined low-cost, high-efficient inverter, peak power tracker and regulator for PV applications," *IEEE Trans. Power Electron.*, vol. 6, pp. 73–82, Jan. 1991.

[15] J. H. R. Enslin, M. S. Wolf, D. B. Snyman, and W. Swiegrs, "Integrated photovoltaic maximum power point tracking converter," *IEEE Trans. Energy Conversion*, vol. 44, pp. 769–773, Dec. 1997.

[16] S. M. Alghuwainem, "Speed control of a PV powered dc motor driving a self-excited three-phase induction generator for maximum utilization efficiency," *IEEE Trans. Energy Conversion*, vol. 11, pp. 768–773, Dec. 1996.

[17] M. A. S. Masoum and H. Dehbonei, "Optimal power point tracking of photovoltaic system under all operating conditions," in *17th Congress of the World Energy Council*, Houston, TX, Sept. 12–18, 1998.

[18] ——, "Design, construction and testing of a voltage-based maximum power point tracker (VMPPT) for small satellite power supply," in *13th Annu. AIAA/USU Conf. Small Satellite*, Aug. 23–26, 1999.

[19] S. M. Alghuwainem, "Matching of a dc motor to a photovoltaic generator using a step-up converter with a current-locked loop," *IEEE Trans. Energy Conversion*, vol. 9, pp. 192–198, Mar. 1994.

Mohammad A. S. Masoum received the B.Sc., M.Sc., and Ph.D. degrees in electrical and computer engineering from the University of Colorado, Boulder, in 1983, 1985, and 1991, respectively.

Currently, he is an Associate Professor at the Iran University of Science and Technology, Tehran. He was a Postdoctoral Fellow at the University of Colorado, Boulder, from 1991 to 1992. From 1983 to 1992, he was a Teaching Assistant, Research Assistant, and Instructor in the Electrical Engineering Department at the University of Colorado.

Hooman Dehbonei received the B.Sc. and M.Sc. degrees in electrical engineering from the Iran University of Science and Technology, Tehran, in 1992 and 1997, respectively. Currently, he is pursuing the Ph.D. degree and is a Research Engineer at the Centre for Renewable Energy and Sustainable Technologies Australia, Perth, designing photovoltaic and aerospace power supply systems.

From 1992 to 1995, he was involved in designing electrical installations with Group 4 Consulting Engineering Company. His research interests include power electronics and renewable energy sources.

Mr. Dehbonei was the recipient of the Best Student Paper Award in 1998.

Ewald F. Fuchs (F'90) received the Dipl.-Ing. degree in electrical engineering from the University of Stuttgart, Stuttgart, Germany, and the Ph.D. degree in electrical engineering from the University of Colorado, Boulder, in 1967 and 1970, respectively.

He is a Professor of electrical engineering at the University of Colorado.